Joint Distributed Beamforming and Backscattering for UAV-Assisted WPSNs

Zhi Mao, *Member, IEEE*, Fengye Hu, *Senior Member, IEEE*, Wen Wu, *Senior Member, IEEE*, Huaqing Wu, *Member, IEEE*, and Xuemin Shen, *Fellow, IEEE*

***Abstract*— This paper studies an unmanned aerial vehicle (UAV)-assisted wireless powered sensor network (WPSN), where sensor nodes of multiple types can simultaneously harvest radio-frequency energy from the UAV and then transmit sensing data by using harvested energy. A joint distributed beamforming (DBF) and backscattering scheme is designed, in which the sensor nodes of one type can perform DBF while the sensor nodes of other types perform distributed backscattering (DBS) to improve the received signal strength. A sum-throughput maximization problem is formulated by jointly optimizing DBF phases, DBS phases, and time allocation (TA), subject to the received signal-to-noise ratio constraints. Since the formulated problem is difficult to be solved due to the tightly coupled optimizing variables, the problem is decoupled into a TA subproblem and a phase optimization subproblem, and then a two-step algorithm is proposed to solve them. Firstly, the closed-form solution for the TA subproblem is derived according to Karush-Kuhn-Tucker conditions. Secondly, based on iterative optimization and one-dimensional search methods, a centralized algorithm is proposed to obtain the optimal solution for the phase optimization subproblem. Moreover, a decentralized algorithm that obtains the suboptimal solution is proposed to reduce the computational complexity. Extensive simulation results validate the effectiveness of the proposed scheme on throughput enhancement.**

***Index Terms*— Wireless powered sensor networks, unmanned aerial vehicle, distributed beamforming, distributed backscattering.**

I. Introduction

IN MASSIVE machine type communications (mMTC) scenarios in the fifth-generation (5G) networks, a massive number of sensor nodes are deployed to support emerging Internet of things (IoT) applications, such as smart agriculture and forest monitoring [2]. To prolong the lifetime of sensor nodes, the wireless powered sensor network (WPSN) is envisioned as a promising paradigm, where sensor nodes harvest ambient radio-frequency (RF) energy from a power transmitter and then transmit their sensing data to an information receiver [3], [4], [5]. However, in the conventional WPSN, power transmitters are usually deployed at fixed locations, which is inflexible to charge scattered sensor nodes in large areas [6].

To overcome this issue, an unmanned aerial vehicle (UAV) can be employed as the mobile power transmitter and information receiver to assist the WPSN [7], [8], [9], [10]. In such UAV-assisted WPSN, a UAV flies from one area to another to charge scattered sensor nodes by using wireless power transfer (WPT) techniques [11], [12]. Then, sensor nodes transmit their sensing data to the UAV by using the harvested energy [13], [14], [15]. However, the throughput performance may still be unsatisfactory due to the impact of the long-distance transmission. Therefore, the UAV has to follow a long trajectory to collect data from scattered sensor nodes, resulting in high time and energy consumption [16], [17], [18].

The distributed beamforming (DBF) technique is a potential approach to enhance the transmission performance, in which the direct link transmission from sensor nodes to the UAV is enhanced by enabling a group of sensor nodes to act as a virtual transmitting antenna array [19], [35]. To enable the DBF, multiple sensor nodes synchronize their carrier frequencies and symbol timing as well as adjust their phases to transmit a message to the UAV [20], [21]. In addition, distributed backscattering (DBS) is another promising technique to enhance transmission performance by using multi-path gains in the indirect link transmission, which can leverage multiple battery-free backscatter nodes to act as passive relay nodes for reflecting the received signals from the transmitting sensor nodes to the UAV [22], [23], [24]. In this way, the received signal strength can be enhanced by effectively leveraging DBF and DBS techniques.

As both the DBF and DBS aim to increase the power in the desired direction and reduce the power scattered in undesired directions, a joint design of them is of great significance to enhance the transmission performance in the UAV-assisted WPSN. It thus motivates us to incorporate the DBF of sensor nodes of one type with the DBS of sensor nodes of other types in a UAV-assisted WPSN with multiple sensor types. In the joint design, a harvest-then-transmit (HTT) protocol is employed in this paper for the WPT and wireless information

Manuscript received 11 February 2022; revised 11 July 2022; accepted 31 August 2022. Date of publication 14 September 2022; date of current version 10 March 2023. This work was supported in part by the Joint Fund for Regional Innovation and Development of the National Natural Science Foundation of China under Grant U21A20445, in part by the National Natural Science Foundation of China under Grant 61671219, in part by the Natural Sciences and Engineering Research Council (NSERC) of Canada, and in part by the Major Key Project of the Peng Cheng Laboratory under Grant PCL2021A09-B2. An earlier version of this paper was presented in part at the IEEE GLOBECOM 2021 [DOI: 10.1109/GLOBECOM46510.2021.9685412]. The associate editor coordinating the review of this article and approving it for publication was Y. Zheng. *(Corresponding author: Fengye Hu.)*

Zhi Mao and Fengye Hu are with the College of Communication Engineering, Jilin University, Changchun 130021, China (e-mail: zhimao17@mails.jlu.edu.cn; hufy@jlu.edu.cn).

Wen Wu is with the Peng Cheng Laboratory, Frontier Research Center, Shenzhen, Guangdong 518055, China (e-mail: wuw02@pcl.ac.cn).

Huaqing Wu is with the Department of Electrical and Software Engineering, University of Calgary, Calgary, AB T2N 1N4, Canada (e-mail: huaqing.wu1@ucalgary.ca).

Xuemin Shen is with the Department of Electrical and Computer Engineering, University of Waterloo, Waterloo, ON N2L 3G1, Canada (e-mail: sshen@uwaterloo.ca).

Color versions of one or more figures in this article are available at https://doi.org/10.1109/TWC.2022.3204915.

Digital Object Identifier 10.1109/TWC.2022.3204915

transfer (WIT) between the UAV and the sensor nodes. The WIT for different types of sensor nodes is performed in a time division multiple access manner. With the DBF and DBS considered among different sensor types, the first challenge is to jointly adjust the DBF and DBS phases to maximize the received signal strength, which incurs a high computational complexity due to multi-dimensional continuous optimization variables. Considering different energy harvesting capabilities of multiple sensor nodes due to channel variation, the second challenge is to optimally allocate the time resource to ensure the received SNR fairness for different sensor types. We aim to address the above issue in this paper and our main contributions are as follows.

- We design a joint DBF and DBS scheme to enhance the uplink transmission performance in the UAV-assisted WPSN. Specifically, the transmitted signals from the sensor nodes of one type are backscattered by the sensor nodes of other types to improve the received signal strength at the UAV.
- We formulate a sum-throughput maximization problem that jointly optimizes DBF phases, DBS phases, and time allocation (TA). To solve the formulated non-convex problem with coupled variables, we propose a two-step algorithm that decomposes it into a TA subproblem and a phase optimization subproblem.
- We derive the closed-form solution for the TA subproblem according to Karush-Kuhn-Tucker (KKT) conditions. For solving the phase optimization subproblem, a centralized algorithm (CA) based on iterative optimization and one-dimensional search is proposed. To reduce the computational complexity, we further propose a decentralized algorithm (DA) that obtains the suboptimal solution.

The remainder of this paper is organized as follows. Related works are presented in Section II. Section III and Section IV describe the system model and the HTT protocol, respectively. In Section V, we formulate a sum-throughput maximization problem and propose a two-step algorithm to solve it. Simulation results are presented in Section VI, and conclusions are drawn in Section VII.

II. Related Work

The UAV-assisted WPSN can be used to enhance the performance of terrestrial wireless communications and prolong the network lifetime. However, the UAV has strict constraints on the battery power and bandwidth [25], [26], [27], [28]. To efficiently leverage the limited UAV resource and prolong service time, there have been some research works on resource allocation optimization for both downlink and uplink transmissions [4], [18], [29], [30], [31], [32], [33], [34]. Xie *et al.* investigated a two-UAV wireless powered communication network (WPCN) with two users for minimum throughput maximization by jointly optimizing the TA, transmit power and UAV trajectory [4]. With the consideration of nonlinear energy harvesting (EH) in a UAV-enabled WPCN, a minimum harvested energy maximization problem was investigated in [18]. To meet various service requirements, a UAV-to-everything communication framework was designed in [29]. An aerial refueling scheme was proposed in [30] for charging UAVs by using WPT techniques. To maximize the sum energy harvested at multiple ground devices, two charging schemes for both 1D and 2D topologies were investigated in [31]. Ye *et al.* studied the optimal TA and hovering time ratio to maximize the sum throughput for UAV-enabled wireless powered IoT networks [32]. Yu *et al.* investigated a multi-objective optimization problem to jointly optimize the sum data rate, sum harvested energy, and UAV's energy consumption over a particular mission period [33]. Considering a wireless powered UAV relay network with non-orthogonal multiple access (NOMA), the performance evaluation of outage probability and ergodic capacity was investigated in [34]. Different from prior works that focus on the resource allocation for independent transmissions of ground devices, our work considers the cooperative transmission of ground devices to enhance uplink transmission performance. Specifically, we propose a novel cooperative transmission scheme, in which the direct and indirect link transmissions are both enhanced.

Very recently, the DBF and DBS are applied as two cooperative transmission technologies in wireless powered networks to enhance throughput performance. The DBF utilizes multiple sensor nodes to act as a virtual antenna array for improving the transmission distance in a specific direction [36], [37]. Xu *et al.* investigated the joint DBF design to maximize the SNR at the receiver in a UAV-assisted WPCN [36]. Feng *et al.* maximized the average data-rate throughput in a delay-tolerant scenario and minimized the transmission outage probability in a delay-sensitive scenario, respectively [37]. The DBS utilizes backscatter nodes to produce constructive multi-path signals to enhance transmission performance [22], [23], [38]. In [22], a throughput maximization problem was investigated by jointly optimizing the TA, power allocation, relays' reflection coefficients and beamforming in a wireless powered backscatter communication network. A backscatter cooperation scheme was proposed in [23] for the NOMA downlink transmission. In [38], Lyu *et al.* studied a throughput maximization problem by optimizing TA in a wireless powered network with a backscatter relay. These works focus on either DBF or DBS for the cooperative transmission. Different from them, our work incorporates the DBF with DBS in a UAV-assisted WPSN. Specifically, a CA and a DA are respectively designed in this work to jointly optimize the DBF and DBS.

III. System Model

A. Network Model

We consider a UAV-assisted WPSN that consists of one hovering UAV and a large number of sensor nodes uniformly deployed in remote areas, as shown in Fig. 1. There are M types of sensor nodes, and the number of sensor nodes in each type is N. We consider that both the sensor nodes and the UAV are equipped with only one antenna and operate over the same frequency band. The hovering UAV is dispatched as an aerial energy transmitter to charge various sensor nodes on the ground. Each sensor node, which has no initial energy in the battery, is equipped with an RF harvester to collect RF energy. In addition, the harvested energy of each sensor node is

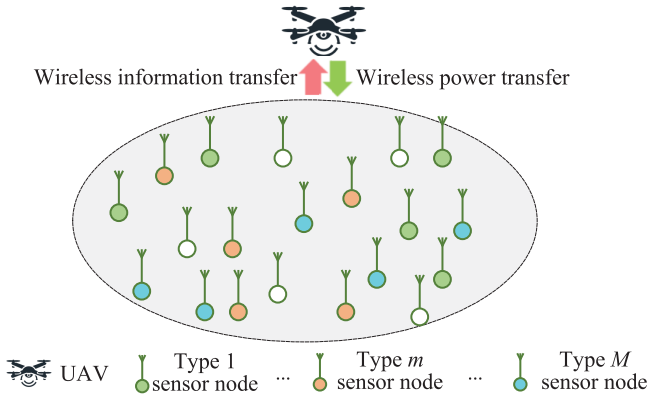

Fig. 1. The UAV-assisted WPSN with various types of single-antenna sensor nodes.

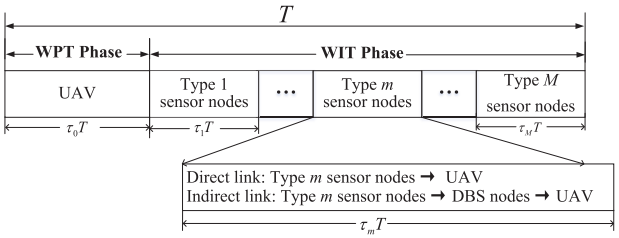

Fig. 2. The transmission protocol in the UAV-assisted WPSN.

used to transmit sensing data to the UAV via DBF. It is noted that the DBF can only be performed among the same-type sensor nodes [36], [39]. When a group of same-type sensor nodes perform DBF to transmit their information, the sensor nodes of all the other sensor types act as backscatter nodes to provide DBS. The sensor nodes can enable the backscatter capability by adjusting the antenna impedance to reflect the received RF signals [22].

The UAV-assisted WPSN adopts the HTT protocol [6] for EH and information transmission between the UAV and sensor nodes, as shown in Fig. 2. In particular, each block transmission time with length T in the HTT protocol is divided into two phases: the WPT phase and the WIT phase. In the WPT phase whose duration is $\tau_0 T$, $0 < \tau_0 \leqslant 1$, all sensor nodes harvest wireless energy from the UAV simultaneously. The WIT phase has a duration of $(1-\tau_0)T$. This phase is divided into M portions for M sensor types, and type m sensor nodes are assigned with duration $\tau_m T$, $0 < \tau_m \leqslant 1$, $\forall m \in \{1, 2, \cdots, M\}$.

To enhance the information transmission performance of type m sensor nodes, a joint DBF and DBS scheme is designed, which is shown in Fig. 3. We consider that the information synchronization has been completed in type m sensor nodes before their information transmission [19], [36]. Then the information of type m sensor nodes can be transmitted by using the harvested energy for DBF. The signals are transmitted via two types of links: the direct link and the indirect link. In the direct link, signals are transmitted from the type m sensor nodes to the UAV directly. In the indirect link, sensor nodes of all the other $M-1$ sensor types provide DBS and reflect signals from type m sensor nodes to the UAV to improve the received SNR. The backscattering coefficient at

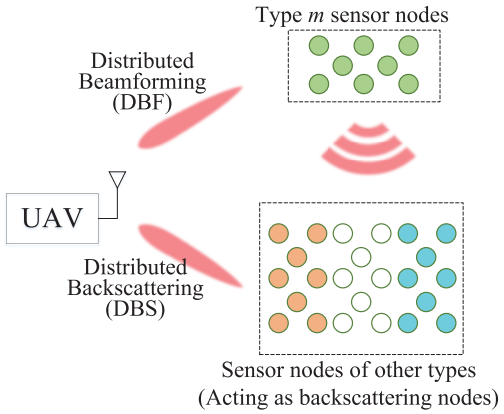

Fig. 3. The joint distributed beamforming and backscattering scheme in the UAV-assisted WPSN.

a cooperative backscatter node is adjusted by tuning the load impedance of its antenna.

B. Channel Model

There are two kinds of wireless channels considered in the network: the air-to-ground (A2G) channel and ground-to-ground (G2G) channel, which are modeled according to [40] and [41], respectively.

A2G channel model: The pathloss in dB between the UAV and a sensor node is modeled as follows [40]:

$$PL_{A2G} = C_{A2G}\log_{10}(d) + 20\log_{10}(f_c) + PL_0^{A2G} + \chi^{\mathrm{A2G}}, \tag{1}$$

where

$$C_{A2G} = \max\{23.9 - 1.8\log_{10}(h_{UT}),\ 20\}, \tag{2}$$

$h_{UT} \in [h_{\min}, h_{\max}]$ is the UAV height in meter, d is the distance in meter between the UAV and a sensor node, f_c is the center carrier frequency in GHz, and PL_0^{A2G} is a related parameter with the constant value. In addition, $h_{\min}$ and $h_{\max}$ are the minimum and maximum heights of the UAV. χ^{A2G} denotes the shadow fading, which follows a log-normal distribution (Gaussian in dB) with zero mean, i.e., $\chi^{\mathrm{A2G}} \sim \mathcal{CN}(0, \sigma^2_{\mathrm{A2G}})$. Here, we have

$$\sigma_{\mathrm{A2G}} = 4.2e^{(-0.0046 h_{UT})},\ h_{UT} \in [h_{\min}, h_{\max}]. \tag{3}$$

G2G channel model: The pathloss in dB between two sensor nodes is modeled as follows [41]:

$$PL_{G2G}(d) = \max\{PL_{FS}(d), PL_{B1}(d)\} + \chi^{\mathrm{G2G}}. \tag{4}$$

Here,

$$\begin{aligned} PL_{FS}(d) &= 20\log_{10}(d) + 20\log_{10}(f_c) + PL_0^{FS}, \\ PL_{B1}(d) &= 43.75\log_{10}(d) + 26.16\log_{10}(f_c) + PL_0^{B1}, \end{aligned} \tag{5}$$

where d is the distance in meter between two sensor nodes, PL_{FS} and PL_{B1} are pathloss in free space and urban microcell scenarios, respectively. In addition, PL_0^{FS} and PL_0^{B1} are two related parameters with constant values. Here, χ^{G2G} denotes the log-normal shadow fading in dB, and $\chi^{\mathrm{G2G}} \sim \mathcal{CN}(0, \sigma^2_{\mathrm{G2G}})$, where $\sigma_{\mathrm{G2G}} = 7$ dB.

Without loss of generality, we consider that the channel reciprocity holds for both G2G and A2G channels. Specifically, wireless channels are quasi-static flat-fading, i.e., channels keep constant in each block, but change independently from one block to another.

C. Energy Harvesting Model

Denote by S_{mn} the n^{th} sensor node of the m^{th} sensor type. Let P_{mn}^{Re} denote the received signal power at sensor node S_{mn}. Since the output of a practical EH circuit is always finite, a nonlinear EH model in [42] with upper boundary M_{mn}^{EH} is adopted in this paper:

$$P_{mn}^{EH} = \frac{\Psi_{mn} - M_{mn}^{EH}\Omega_{mn}}{1-\Omega_{mn}}, \tag{6}$$

where

$$\Omega_{mn} = \frac{1}{1+e^{a_{mn}b_{mn}}}, \quad \Psi_{mn} = \frac{M_{mn}^{EH}}{1+e^{-a_{mn}(P_{mn}^{Re}-b_{mn})}}, \tag{7}$$

P_{mn}^{EH} is the practical EH power at sensor node S_{mn}, which is a logistic function with respect to the received signal power P_{mn}^{Re} [42]. Here, a_{mn} and b_{mn} are parameters related to the detailed EH circuit. M_{mn}^{EH} is the maximum output of the EH circuit at sensor node S_{mn}.

IV. Harvest-Then-Transmit Protocol

The HTT protocol consists of two phases, which are presented in the following two subsections.

A. Wireless Power Transfer Phase

During the WPT phase, the UAV charges all sensor nodes simultaneously through WPT techniques. The received signal at sensor node S_{mn} is given by

$$y_{mn}^{s} = \sqrt{P_a}h_{mn}x_a + z_{mn}, \tag{8}$$

where x_a and P_a are the normalized transmitted signal and the transmit power of the UAV, respectively. $h_{mn} \in \mathbb{C}^{1\times 1}$ denotes the channel coefficient from the UAV to sensor node S_{mn}. In addition, $z_{mn} \sim \mathcal{CN}(0,\sigma_{mn}^2)$ is the additive white Gaussian noise (AWGN) at the receiving antenna of sensor node S_{mn}. The received signal power at sensor node S_{mn} can be obtained by

$$P_{mn}^{Re} = \mathbb{E}\left[\left|y_{mn}^{s}\right|^2\right] = \left|\sqrt{P_a}h_{mn}\right|^2 + \sigma_{mn}^2 \approx P_a\left|h_{mn}\right|^2. \tag{9}$$

Substituting Eq. (9) into Eq. (6), the practical EH power P_{mn}^{EH} can be obtained. Then the amount of energy harvested at sensor node S_{mn} in this phase can be expressed as

$$E_{mn} = P_{mn}^{EH}\tau_0 T. \tag{10}$$

B. Wireless Information Transfer Phase

The WIT phase is divided into M portions unequally for M sensor types, as shown in Fig. 2. Within the time duration of $\tau_m T$ assigned to type m sensor nodes, all the type m sensor nodes exhaust the harvested energy to transmit their information to the UAV. The transmitted signal at sensor node S_{mn} can be expressed as:

$$x_{mn} = \sqrt{\frac{E_{mn}}{\tau_m T}}e^{j\theta_{mn}^{Tx}}s_m, \tag{11}$$

where θ_{mn}^{Tx} is the phase of transmitted signal at sensor node S_{mn}, and s_m is the baseband transmitted signal of the information of type m sensor nodes. Let $\boldsymbol{x}_m = [x_{m1},\cdots,x_{mn},\cdots,x_{mN}]^T$ denote the DBF vector for type m sensor nodes. Then the received signal at the UAV can be expressed as

$$y_m^a = (\underbrace{\boldsymbol{g}_{d_m}^T}_{\text{Direct link}} + \underbrace{\boldsymbol{g}_{r_m}^T\boldsymbol{\Phi}_m\boldsymbol{H}_m}_{\text{Indirect link}})\,\boldsymbol{x}_m + z', \tag{12}$$

where $\boldsymbol{g}_{d_m} \in \mathbb{C}^{N\times 1}$ is the channel vector from the type m sensor nodes to the UAV. Although there are two links, the transmission signals are identical. Thus, the one-antenna AP receives the signal in two paths and combines them by using the equal gain combining method [22].

Considering the channel reciprocity, we have $\boldsymbol{g}_{d_m} = [h_{m1},\cdots,h_{mn},\cdots,h_{mN}]^T$. $\boldsymbol{g}_{r_m} \in \mathbb{C}^{K\times 1}$ is the channel vector from the backscatter nodes to the UAV, where $K = N(M-1)$ denotes the number of backscatter nodes.[1] $\boldsymbol{H}_m \in \mathbb{C}^{K\times N}$ is the channel matrix from the type m sensor nodes to the backscatter nodes. $\boldsymbol{\Phi}_m \in \mathbb{C}^{K\times K} = \text{diag}(\beta_{m1}e^{j\theta_{m1}^{DB}},\cdots,\beta_{mk}e^{j\theta_{mk}^{DB}},\cdots,\beta_{mK}e^{j\theta_{mK}^{DB}})$ denotes the backscattering coefficient diagonal matrix of the backscatter nodes, where $0 \leqslant \beta_{mk} \leqslant 1$ and $-\pi \leqslant \theta_{mk}^{DB} \leqslant \pi$ denote the backscattering amplitude and the phase at backscatter node k, respectively. We set $\forall\beta_{mk} = 1$ in this paper for simplicity in derivations, but the scheme proposed in this paper can be easily extended to the case with arbitrary values of $\beta_{mk} \in [0,1]$. $z' \sim \mathcal{CN}(0,\sigma^2)$ denotes the AWGN at the receiving antenna of the UAV. Thus, the received SNR at the UAV from type m sensor nodes can be expressed as:

$$\begin{aligned}\gamma_m &= \frac{\left|\left(\boldsymbol{g}_{d_m}^T + \boldsymbol{g}_{r_m}^T\boldsymbol{\Phi}_m\boldsymbol{H}_m\right)\boldsymbol{x}_m\right|^2}{\sigma^2} \\ &= \frac{\left|\left(\boldsymbol{g}_{d_m}^T\boldsymbol{\Lambda}_m + \boldsymbol{g}_{r_m}^T\boldsymbol{\Phi}_m\boldsymbol{H}_m\boldsymbol{\Lambda}_m\right)\boldsymbol{\omega}_m'\right|^2}{\sigma^2}\frac{\tau_0}{\tau_m},\end{aligned} \tag{13}$$

where

$$\begin{aligned}\boldsymbol{\Lambda}_m &= \text{diag}\left\{\sqrt{P_{m1}^{EH}},\cdots,\sqrt{P_{mn}^{EH}},\cdots,\sqrt{P_{mN}^{EH}}\right\}, \\ \boldsymbol{\omega}_m' &= \left[e^{j\theta_{m1}^{Tx}},\cdots,e^{j\theta_{mn}^{Tx}},\cdots e^{j\theta_{mN}^{Tx}}\right]^T \in \mathbb{C}^{N\times 1}.\end{aligned} \tag{14}$$

We define $\gamma_m' = \frac{\left|\left(\boldsymbol{g}_{d_m}^T\boldsymbol{\Lambda}_m + \boldsymbol{g}_{r_m}^T\boldsymbol{\Phi}_m\boldsymbol{H}_m\boldsymbol{\Lambda}_m\right)\boldsymbol{\omega}_m'\right|^2}{\sigma^2}$ as the unit SNR achieved by type m sensor nodes, then we have

$$\gamma_m = \gamma_m'\frac{\tau_0}{\tau_m}. \tag{15}$$

[1]Although the number of sensor nodes in each type is assumed to be the same in this paper, the proposed scheme can be directly applied to the networks with various numbers in different sensor types by using $K = \sum_{i=1,i\neq m}^{M} N_i$ as the number of backscatter nodes for information transmission of type m sensor nodes, where N_i is the number of sensor nodes in type i sensor nodes.

The throughput of type m sensor nodes in bits/second/Hz (bps/Hz) can be expressed as:

$$R_m = \tau_m \log_2 (1 + \gamma_m). \tag{16}$$

V. Problem Formulation and Optimization Strategies

In this section, the sum-throughput maximization problem of the UAV-assisted WPSN with M sensor types is formulated. Let $\boldsymbol{\theta}_m^{Tx} = [\theta_{m1}^{Tx}, \cdots, \theta_{mn}^{Tx}, \cdots, \theta_{mN}^{Tx}]^T$ and define a real matrix $\boldsymbol{\Theta}^{Tx} = [\boldsymbol{\theta}_1^{Tx}, \cdots, \boldsymbol{\theta}_m^{Tx}, \cdots, \boldsymbol{\theta}_M^{Tx}]$ as the DBF phase matrix. Let $\boldsymbol{\theta}_m^{DB} = [\theta_{m1}^{DB}, \cdots, \theta_{mk}^{DB}, \cdots, \theta_{mK}^{DB}]^T$ and define a real matrix $\boldsymbol{\Theta}^{DB} = [\boldsymbol{\theta}_1^{DB}, \cdots, \boldsymbol{\theta}_m^{DB}, \cdots, \boldsymbol{\theta}_M^{DB}]$ as the DBS phase matrix. $\boldsymbol{\tau} = [\tau_0, \tau_1, \cdots, \tau_M]^T$ represents the optimizing variables of TA. Then, the sum-throughput maximization problem subject to the received SNR constraints can be expressed as:

$$\begin{aligned} \text{P1}: \max_{\boldsymbol{\tau}, \boldsymbol{\Theta}^{Tx}, \boldsymbol{\Theta}^{DB}} \quad & \sum_{m=1}^{M} \tau_m \log_2 \left(1 + \gamma_m' \left(\boldsymbol{\theta}_m^{Tx}, \boldsymbol{\theta}_m^{DB}\right) \frac{\tau_0}{\tau_m}\right), \\ \text{s.t.} \quad & \tau_0 + \sum_{m=1}^{M} \tau_m = 1, \\ & \gamma_m \geqslant \gamma_0. \end{aligned} \tag{17}$$

The above optimization problem is non-convex due to the coupled variables in the objective function. To solve the complicated problem with coupled variables, we propose an optimization algorithm with two steps: the TA optimization and the phase optimization. The detailed procedure of the proposed two-step algorithm is given in the following two subsections.

A. Time Allocation Optimization

In this subsection, we derive the closed-form expressions of the TA solution. Note that $\gamma_m'(\boldsymbol{\theta}_m^{Tx}, \boldsymbol{\theta}_m^{DB})$ in the objective function of problem P1 is a function of $\boldsymbol{\theta}_m^{Tx}$ and $\boldsymbol{\theta}_m^{DB}$, while it is unrelated to $\boldsymbol{\tau}$. For a set of given $\boldsymbol{\theta}_m^{Tx}$ and $\boldsymbol{\theta}_m^{DB}$, problem P1 is reduced as:

$$\text{P1.1}: \max_{\boldsymbol{\tau}} \quad \sum_{m=1}^{M} \tau_m \log_2(1 + \gamma_m' \frac{\tau_0}{\tau_m}), \tag{18a}$$

$$\text{s.t.} \quad \tau_0 + \sum_{m=1}^{M} \tau_m = 1, \tag{18b}$$

$$\gamma_m' \frac{\tau_0}{\tau_m} \geqslant \gamma_0. \tag{18c}$$

The objective function of problem P1.1 is the sum of perspective functions of $\log_2(1 + \gamma_m' \tau_0)$ that is a concave function. According to the preserve convexity property [43], the objective function is also concave. In addition, all the constraints of problem P1.1 are linear. Thus, problem P1.1 is a convex optimization problem and can be solved by using convex optimization tools. However, excessive computing is required to find the optimal solution in the feasible set. To overcome this issue, we first derive the optimal SNR for problem P1.1. Then we derive the closed-form expressions of the TA solution based on the obtained optimal SNR and TA constraints.

*1) **Optimal SNR**:* The optimal SNR for problem P1.1 is obtained based on convex optimization techniques. To obtain the optimal SNR, we first ignore the SNR constraints to derive an ideal SNR solution according to Karush-Kuhn-Tucker (KKT) conditions. Then the obtained ideal SNR solution is compared with the SNR threshold in constraint (18c) to obtain the optimal SNR for problem P1.1. The Lagrange dual function of objective function (18a) with constraint (18b) is given as:

$$L = \sum_{m=1}^{M} \tau_m \log_2(1 + \gamma_m' \frac{\tau_0}{\tau_m}) - \mu(\tau_0 + \sum_{m=1}^{M} \tau_m - 1), \tag{19}$$

where μ is the Lagrangian multiplier associated with constraint (18b). According to KKT conditions, we have

$$\frac{\partial L}{\partial \tau_0}(\boldsymbol{\tau}^*) = \frac{1}{\ln 2} \sum_{m=1}^{M} \frac{\gamma_m'}{1 + \gamma_m} - \mu = 0, \tag{20a}$$

$$\frac{\partial L}{\partial \tau_m}(\boldsymbol{\tau}^*) = \frac{1}{\ln 2} \left(\ln(1 + \gamma_m) - \frac{\gamma_m}{1 + \gamma_m}\right) - \mu = 0, \tag{20b}$$

where $\gamma_m = \gamma_m' \frac{\tau_0}{\tau_m}$. By combining Eq. (20a) with Eq. (20b) and eliminating variable μ, we have

$$f(\gamma_m) = \sum_{i=1}^{M} \frac{\gamma_i'}{1 + \gamma_i}, \ \forall m = 1, 2, \cdots, M, \tag{21}$$

where $f(x) = \ln(1 + x) - \frac{x}{1+x}, \ x > 0$ is a monotonically increasing function. Because $f(\gamma_1) = \cdots = f(\gamma_M)$, we have $\gamma_1 = \cdots = \gamma_M = \bar{\gamma}$. Thus, a common SNR $\bar{\gamma}$ will be achieved when the sum throughput is maximized without considering constraint (18c). With the common SNR, Eq. (21) can be rewritten as

$$\ln(1 + \bar{\gamma}) - \frac{\bar{\gamma}}{1 + \bar{\gamma}} = \frac{\sum_{i=1}^{M} \gamma_i'}{1 + \bar{\gamma}}, \tag{22a}$$

$$\Rightarrow \ \frac{\sum_{i=1}^{M} \gamma_i' - 1}{1 + \bar{\gamma}} e^{\frac{-1 + \sum_{i=1}^{M} \gamma_i'}{1 + \bar{\gamma}}} = \frac{(\sum_{i=1}^{M} \gamma_i' - 1)}{e}, \tag{22b}$$

$$\Rightarrow \ \omega(\bar{\gamma}) e^{\omega(\bar{\gamma})} = \frac{(\sum_{i=1}^{M} \gamma_i' - 1)}{e}, \tag{22c}$$

where $\omega(\bar{\gamma}) = \frac{\sum_{i=1}^{M} \gamma_i' - 1}{1 + \bar{\gamma}}$. By using the Lambert W function, the value of ω in Eq. (22c) can be obtained and denoted by ω^*, then we have

$$\bar{\gamma} = \frac{\sum_{i=1}^{M} \gamma_i' - 1}{\omega^*} - 1. \tag{23}$$

However, the value of $\bar{\gamma}$ may violate constraint (18c). To avoid the contradiction, the optimal SNR of problem P1.1 can be expressed as:

$$\gamma^* = \max\{\bar{\gamma}, \gamma_0\}. \tag{24}$$

Lemma 1: $\gamma_1 = \gamma_2 = \cdots = \gamma_M$ holds when the optimal TA solution of problem P1.1 is achieved.

Proof: Please refer to Appendix A.

*2) **Optimal TA**:* Substituting the value of obtained optimal SNR solution into Eq. (15), we have

$$\tau_m = \frac{\gamma'_m}{\gamma^*}\tau_0. \tag{25}$$

Substituting Eq. (25) into Eq. (18b), we can get the closed-form expressions of the optimal TA solution as follows:

$$\begin{cases} \tau_0^* = \dfrac{\gamma^*}{\gamma^* + \sum_{i=1}^{M} \gamma'_i}, \\ \tau_m^* = \dfrac{\gamma'_m}{\gamma^* + \sum_{i=1}^{M} \gamma'_i}, \quad m = 1, 2, \cdots, M. \end{cases} \tag{26}$$

B. Phase Optimization

The phase solution consists DBF and DBS phase solutions. The DBF phase solution is obtained by applying the maximum-ratio transmission (MRT) method. The DBS phase solution can be obtained in centralized or decentralized ways. Thus, a CA and a DA are designed respectively for the phase optimization.

After substituting the TA solution in Eq. (26) into P1, we have

$$\max_{\boldsymbol{\Theta}^{Tx}, \boldsymbol{\Theta}^{DB}} \quad \frac{\sum_{m=1}^{M} \gamma'_m \left(\boldsymbol{\theta}_m^{Tx}, \boldsymbol{\theta}_m^{DB}\right)}{\gamma^* + \sum_{m=1}^{M} \gamma'_m \left(\boldsymbol{\theta}_m^{Tx}, \boldsymbol{\theta}_m^{DB}\right)} \log_2 (1 + \gamma^*). \tag{27}$$

The above problem can be equivalently changed into a set of optimization problems to maximize γ'_m, $\forall m = 1, 2, \cdots, M$. Each of them can be expressed as:

$$\begin{aligned} \text{P1.2}: \max_{\boldsymbol{\theta}_m^{Tx}, \boldsymbol{\theta}_m^{DB}} \quad & \frac{\left|\left(\boldsymbol{g}_{d_m}^T \boldsymbol{\Lambda}_m + \boldsymbol{g}_{r_m}^T \boldsymbol{\Phi}_m \boldsymbol{H}_m \boldsymbol{\Lambda}_m\right) \boldsymbol{\omega}'_m\right|^2}{\sigma^2} \\ \text{s.t.} \quad & -\pi \leqslant \theta_{mn}^{Tx} \leqslant \pi, \, \forall n \in \{1, 2, \cdots, N\}, \\ & -\pi \leqslant \theta_{mk}^{DB} \leqslant \pi, \, \forall k \in \{1, 2, \cdots, K\}. \end{aligned} \tag{28}$$

Problem P1.2 is a joint DBF and DBS phase optimization problem. According to the MRT method, the optimal solution of $\boldsymbol{\theta}_m^{Tx}$ can be denoted by $\boldsymbol{\theta}_m^{Tx*} = \arg\left(\boldsymbol{\omega}_m^{MRT}\right)$, where $\boldsymbol{\omega}_m^{MRT}$ is the MRT beamforming vector and can be expressed as:

$$\boldsymbol{\omega}_m^{MRT} = \frac{\left(\boldsymbol{g}_{d_m}^T \boldsymbol{\Lambda}_m + \boldsymbol{g}_{r_m}^T \boldsymbol{\Phi}_m \boldsymbol{H}_m \boldsymbol{\Lambda}_m\right)^H}{\left\|\boldsymbol{g}_{d_m}^T \boldsymbol{\Lambda}_m + \boldsymbol{g}_{r_m}^T \boldsymbol{\Phi}_m \boldsymbol{H}_m \boldsymbol{\Lambda}_m\right\|}. \tag{29}$$

Substituting $\boldsymbol{\theta}_m^{Tx*}$ into problem P1.2 and simplifying the expression, we have

$$\begin{aligned} \text{P1.2.1}: \max_{\boldsymbol{\theta}_m^{DB}} \quad & \left\|\boldsymbol{g}_{d_m}^T \boldsymbol{\Lambda}_m + \boldsymbol{u}_m^T \boldsymbol{\Psi}_m\right\|_1, \\ \text{s.t.} \quad & -\pi \leqslant \theta_{mk}^{DB} \leqslant \pi, \, \forall k \in \{1, 2, \cdots, K\}, \end{aligned} \tag{30}$$

where

$$\begin{aligned} \boldsymbol{\Psi}_m &= \text{diag}(\boldsymbol{g}_{r_m}^T) \boldsymbol{H}_m \boldsymbol{\Lambda}_m, \\ \boldsymbol{u}_m &= \left[e^{j\theta_{m1}^{DB}}, \cdots, e^{j\theta_{mk}^{DB}}, \cdots, e^{j\theta_{mK}^{DB}}\right]^T. \end{aligned} \tag{31}$$

Algorithm 1 Centralized Algorithm for P1.2

Input: Global CSI, $\left\{P_{m1}^{EH}, \cdots, P_{mN}^{EH}\right\}$;
Output: The DBS phase vector $\left(\boldsymbol{\theta}_m^{DB}\right)^*$ and the DBF phase vector $\left(\boldsymbol{\theta}_m^{Tx}\right)^*$.

```
// Backscattering phases optimization
```
Initialize $i = 0$, $\boldsymbol{\theta}^{(i)} = \mathbf{0}^{K \times 1}$, δ;
$\gamma_m'^{(i)} = \gamma'_m(\boldsymbol{\theta}^{(i)})$;
while $\left|\gamma_m'^{(i)} - \gamma_m'^{(i-1)}\right| \geqslant \delta$ **do**
  $i = i + 1$;
  for $k \in \{1, 2, \cdots, K\}$ **do**
    Set $\boldsymbol{\Theta}_k = \left\{\theta_{k'}^{(i-1)}\right\}, \forall k' \neq k$;
    Set a feasible set $\theta_{tmp} \in [-\pi, \pi]$;
    $\theta_k^{(i)} = \arg\max \gamma'_m(\theta_{tmp}, \boldsymbol{\Theta}_k)$;
  end
  $\boldsymbol{\theta}^{(i)} = [\theta_1^{(i)}, \cdots, \theta_K^{(i)}]^T$;
  $\gamma_m'^{(i)} = \gamma'_m\left(\boldsymbol{\theta}^{(i)}\right)$;
end
$\left(\boldsymbol{\theta}_m^{DB}\right)^* = \boldsymbol{\theta}^{(i)}$;
```
// Transmitting phases optimization
```
Calculate $\boldsymbol{\omega}_m^{MRT}$ by using Eq. (29);
$\left(\boldsymbol{\theta}_m^{Tx}\right)^* = \arg(\boldsymbol{\omega}_m^{MRT})$;
Return $\left(\boldsymbol{\theta}_m^{DB}\right)^*$ and $\left(\boldsymbol{\theta}_m^{Tx}\right)^*$.

To solve the phase optimization problem, we design a CA and a DA respectively in the following two parts. The CA is designed to obtain the optimal solution to the problem. Considering the computational complexity to implement the CA, a DA is designed to obtain the low-complexity suboptimal solution with closed-form expressions.

*1) **Centralized Algorithm**:* We propose a CA by jointly applying the one-dimensional search and iterative optimization to find the optimal DBS phase solution. The expression of objective function in problem P1.2.1 can be rewritten as:

$$\begin{aligned} &\left\|\boldsymbol{g}_{d_m}^T \boldsymbol{\Lambda}_m + \boldsymbol{u}_m^T \boldsymbol{\Psi}_m\right\|_1 \\ &\quad = \left\| e^{j\theta_{mk}^{DB}} \boldsymbol{\psi}_{mk} + \sum_{i=1, i \neq k}^{K} e^{j\theta_{mi}^{DB}} \boldsymbol{\psi}_{mi} + \boldsymbol{g}_{d_m}^T \boldsymbol{\Lambda}_m \right\|_1, \end{aligned} \tag{32}$$

where $\boldsymbol{\psi}_{mk}$ is the k^{th} row of matrix $\boldsymbol{\Psi}_m$. It is observed that the function of $\gamma'_m(\theta_{mk}^{DB})$ is a successive and periodical function with period 2π over θ_{mk}^{DB}, $\forall k \in \{1, 2, \cdots, K\}$. For a given initial $\boldsymbol{\theta}_m^{DB}$, the value of each θ_{mk}^{DB}, $\forall k \in \{1, 2, \cdots, K\}$ can be updated to maximize $\gamma'_m(\theta_{mk}^{DB})$ by using one-dimensional search method such as Höpfinger golden section search method [44]. After updating each θ_{mk}^{DB}, $\forall k \in \{1, 2, \cdots, K\}$ in an iteration, the updated $\boldsymbol{\theta}_m^{DB}$ can be regarded as the initial value in a new iteration. Finally, iterations stop when a tolerant error is reached. To summarize, a CA to solve problem P1.2 is given in Algorithm 1 in detail.

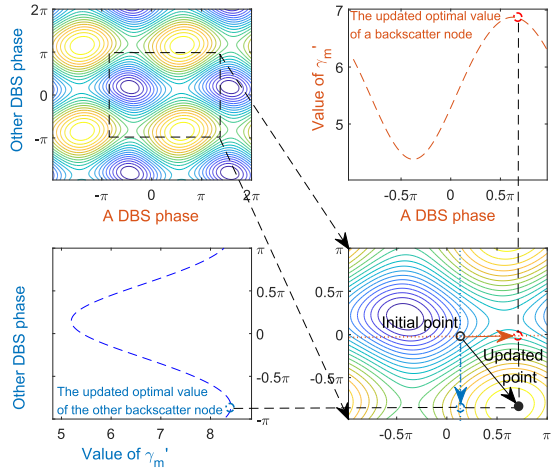

Fig. 4. The value of γ_m' versus different backscattering phases of two backscatters.

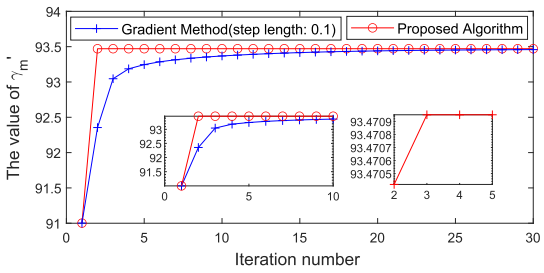

(a) The convergence performance comparison between the proposed algorithm and the traditional gradient method.

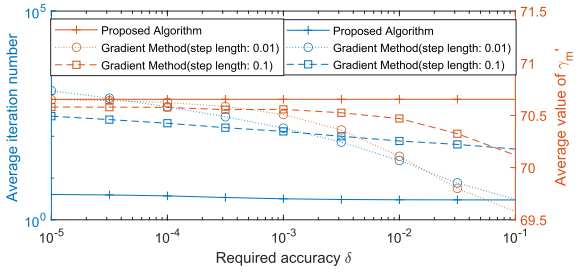

(b) The impact of the tolerant error.

Fig. 5. The performance comparison between the proposed algorithm and the conventional gradient algorithm.

Figure 4 shows an iteration of the proposed CA in a UAV-assisted WPSN with two backscatter nodes. When it is extended to the case with more than two backscatter nodes, the phase of a backscatter node is optimized by fixing all the phases at the other backscatter nodes. Fig. 5 shows the detailed performance comparison between the proposed CA and the conventional gradient algorithm to find the optimal solution. As shown in Fig. 5(a), the proposed algorithm requires fewer iterations to find the optimal solution than the conventional gradient algorithm. This observation validates the effectiveness of the proposed algorithm because it can find the optimal solution faster than the conventional gradient algorithm. The average number of iterations required to achieve a desired tolerant error is shown in Fig. 5(b). It is observed that the conventional gradient algorithm requires a significantly larger number of iterations than the proposed algorithm for the case with a low tolerant error. For the case with a high tolerant error, the conventional gradient algorithm achieves negligible improvement in each iteration, which results in the early stop of iteration and unsatisfactory value of γ_m'. Specifically, The proposed algorithm can find a better solution as compared to the conventional gradient algorithm because of the achieved higher SNR. In addition, the performance of the conventional gradient algorithm is highly dependent on the step size.[2] However, it is difficult to adaptively regulate the step size in iterations, which results in serious inefficiency. The improper step size may result in the mismatch or excessive iterations [43]. Instead of utilizing the step size in the conventional gradient algorithm for computing updated values, the proposed algorithm directly uses the one-dimensional search to find the updated value in an iteration. Then, the number of iterations is effectively decreased compared with the conventional gradient algorithm.

Computational complexity analysis: The proposed CA is designed based on iterative optimization and one-dimensional search methods. Specifically, there are $K = (M-1)N$ one-dimensional searches in each iteration, and the computational complexity of the adopted Höpfinger golden section search method is $\mathcal{O}(\log(1/\epsilon))$, given the solution accuracy $\epsilon > 0$. Thus, the computational complexity of the proposed CA is $\mathcal{O}(N_{ite}K\log(1/\epsilon))$, where N_{ite} denotes the number of iterations before reaching the stopping criteria.

Algorithm implementation: To implement the proposed CA in the UAV-assisted WPSN, the UAV acts as the centralized node to calculate the beamforming vector based on the global CSI, and then sends the results to sensor nodes. The CSI is required for executing the algorithm, and such CSI is reported to the UAV by sensor nodes [22], [45], [46].

*2) **Decentralized Algorithm**:* Considering the communication cost for obtaining global CSI and computational complexity, we design a DA with low complexity. To avoid signal cancellation of received signals at the UAV, we aim to design the DA to make the phases of received signals at the UAV from direct links and indirect links the same, i.e.,

$$\arg(\boldsymbol{g}_{d_m}^T \boldsymbol{\Lambda}_m) = \arg(\boldsymbol{u}_m \boldsymbol{\Psi}_m). \tag{33}$$

For simplicity, we consider that $\arg(\boldsymbol{g}_{d_m}^T \boldsymbol{\Lambda}_m) = \arg(\boldsymbol{u}_m \boldsymbol{\Psi}_m) = [0, \cdots, 0, \cdots, 0]^{N\times 1}$. To achieve that, the transmitting phase at sensor node S_{mn} can be expressed as

$$\theta_{mn}^{Tx*} = \arg(h_{mn}^H) = -\arg(h_{mn}). \tag{34}$$

According to Eq. (11), the transmitted signal at sensor node S_{mn} can be expressed as:

$$x_{mn}^* = \sqrt{\frac{E_{mn}}{\tau_m T}} e^{j\theta_{mn}^{Tx*}} s_m = \frac{\tau_0}{\tau_m} \sqrt{P_{mn}^{EH}} e^{j\theta_{mn}^{Tx*}} s_m. \tag{35}$$

To compute the backscattering phase by using the DA, backscatter node k requires the phase information of the

[2] An iteration in the conventional gradient algorithm can be expressed by $\theta_1 = \theta_0 + \alpha\Delta\theta$, where θ_1, θ_0, $\Delta\theta$, and α denote the updated value, initial value, gradient at the initial value and step size, respectively.

Algorithm 2 Decentralized Algorithm for P1.2

Input: Local CSI, $\left\{P_{m1}^{EH}, \cdots, P_{mN}^{EH}\right\}$;

Output: The DBS phase vector $\left(\boldsymbol{\theta}_m^{DB}\right)^*$ and the DBF phase vector $\left(\boldsymbol{\theta}_m^{Tx}\right)^*$.

// Transmitting phases optimization

for each $n \in \{1, \cdots, N\}$ **do**

  $\theta_{mn}^{Tx} = -\arg(h_{mn})$;

end

$\left(\boldsymbol{\theta}_m^{Tx}\right)^* = [\theta_{m1}^{Tx}, \cdots, \theta_{mN}^{Tx}]^T$;

// Backscattering phases optimization

for each $k \in \{1, \cdots, K\}$ **do**

  $y^{tmp} = \sum_{n=1}^{N} \sqrt{P_{mn}^{EH}} e^{j\theta_{mn}^{Tx}} h_{mn,k}$;

  $\theta_{mk}^{DB} = -\arg(y^{tmp}) - \arg(h_{ak})$;

end

$\left(\boldsymbol{\theta}_m^{DB}\right)^* = [\theta_{m1}^{DB}, \cdots, \theta_{mK}^{DB}]^T$;

Return $\left(\boldsymbol{\theta}_m^{DB}\right)^*$ and $\left(\boldsymbol{\theta}_m^{Tx}\right)^*$.

incident signal and the CSI from itself to the UAV. The incident signal at backscatter node k can be represented by

$$y_{in}^{(k)} = \frac{\tau_0}{\tau_m} \left(\sum_{n=1}^{N} \sqrt{P_{mn}^{EH}} e^{j\theta_{mn}^{Tx*}} h_{mn,k} \right) s_m, \tag{36}$$

where $h_{mn,k} \in \mathbb{C}^{1\times 1}$ denotes the channel coefficient from sensor node S_{mn} to backscatter node k. Since $\arg(y_{in}^{(k)}) = \arg((\sum_{n=1}^{N} \sqrt{P_{mn}^{EH}} e^{j\theta_{mn}^{Tx*}} h_{mn,k}) s_m)$, TA optimization does not affect the computation for optimal backscattering phases. To maximize the received signal strength at the UAV, backscatter node k adjusts its phase to ensure that the phase of the received signals at the UAV from arbitrary backscatter node k is the same as those in direct links. To achieve that, the backscattering phase at backscatter node k can be expressed as

$$\theta_{mk}^{DB*} = \arg(y_{in}^{(k)H} h_{ak}^H) = -\arg(y_{in}^{(k)}) - \arg(h_{ak}), \tag{37}$$

where $h_{ak} \in \mathbb{C}^{1\times 1}$ is the channel coefficient from backscatter node k to the UAV.

To achieve the above distributed optimization, a DA is given in Algorithm 2 in detail.

Computational complexity analysis: The computational complexity of the proposed DA can be shown to be $\mathcal{O}(1)$ since the DBF and DBS solution is derived in closed-form expressions, i.e., (34) and (37).

Algorithm implementation: To implement the proposed DA, the UAV first broadcasts a pilot signal, and the channel estimation is completed at each sensor node S_{mn} to obtain the knowledge of $\arg(h_{mn})$. In addition, backscatter node k obtains the knowledge of $\arg(h_{ak})$ at the same time. With the knowledge of $\arg(h_{mn})$, sensor node S_{mn} can compute the transmitting phase θ_{mn}^{Tx*} based on Eq. (34). Meanwhile, backscatter node k performs incident signal estimation and get the knowledge of $\arg(y_{in}^{(k)})$. Then, the backscatter node k computes the backscattering phase θ_{mk}^{DB*} based on Eq. (37). Compared with the CA, the communication cost of the DA is effectively reduced because there is no need to obtain the global CSI at the UAV. Thus, there is no need to make information exchange among sensor nodes.

To this end, the initial optimization problem P1 can be solved by using our proposed two-step algorithm. Firstly, the joint DBF and DBS phases are optimized by using the proposed CA or DA. Based on the obtained phases, the TA ratios are optimized according to the closed-form expressions in Eq. (26).

VI. Simulation Results

A. Simulation Setup

In this section, extensive simulation results in a UAV-assisted WPSN with multiple sensor types are provided. The noise power of AWGN at the receiving antenna is $\sigma^2 = -100\,\text{dBm}$ [4]. Sensor nodes are distributed in a circle with radius R^{loc} and the locations of sensor nodes are uniformly distributed. In addition, the UAV is hovering above the circle center with height D_H. In the non-linear EH model, we have $a_{mn} = 150$, $b_{mn} = 0.014$, and $M_{mn}^{EH} = 24\,\text{mW}$, $\forall m, n$ [42]. In the channel model, we have $PL_0^{A2G} = 32.44\,\text{dB}$, $PL_0^{FS} = 32.42\,\text{dB}$, $PL_0^{B1} = 17.36\,\text{dB}$, $h_{\min} = 10\,\text{m}$ and $h_{\max} = 300\,\text{m}$ [40], [41]. In addition, the center carrier frequency is set as 915 MHz [31]. Simulation results are averaged over 10, 000 trials with different channel fading and sensor nodes' locations. Based on the obtained optimal solution in Section V, we compare the proposed scheme with the following benchmark schemes:

- **Equal TA (ETA)-based DBF scheme**: In this scheme, the time for WPT and WIT of each sensor type is allocated equally, i.e., $\tau_m = 1/(M+1)$, $\forall m = 0, 1, \cdots, M$. In this case, the received SNR at the UAV may violate constraint (18c). In addition, only DBF for direct link transmission is considered, and γ_m' is set to $\left|\boldsymbol{g}_{d_m}^T \boldsymbol{\Lambda}_m\right|^2 / \sigma^2$.
- **Optimal TA (OTA)-based DBF scheme**: In this scheme, the time for WPT and WIT of each sensor type is allocated based on Eq. (26). In addition, only DBF for direct link transmission is considered, and the DBF phase is optimized by using Eq. (34).
- **OTA-based DBF scheme with random-phase DBS**: In this scheme, the time for WPT and WIT of each sensor type is allocated based on Eq. (26). The DBF phase is optimized by using Eq. (34), and the DBS phase follows the uniformly random distribution.

B. SNR Performance

According to ***Lemma 1***, the TA optimization in our proposed scheme is able to achieve a common SNR. However, in schemes without TA optimization, the values of different γ_m's are different because of equal TA and unequal γ_m'. Considering the communication fairness, the value of $\min\{\gamma_m\}$ is used to represent the SNR performance of schemes without TA optimization.

Figure 6 shows the impact of the radius of the simulated area R^{loc} on the average SNR performance with $M = 6$,

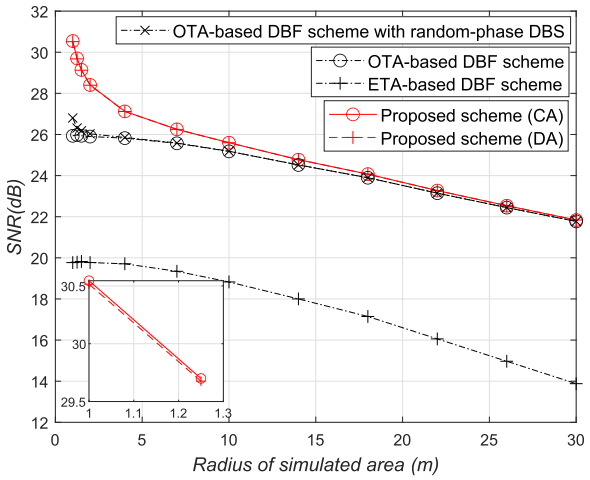

Fig. 6. The average SNR performance of different schemes versus the coverage radius.

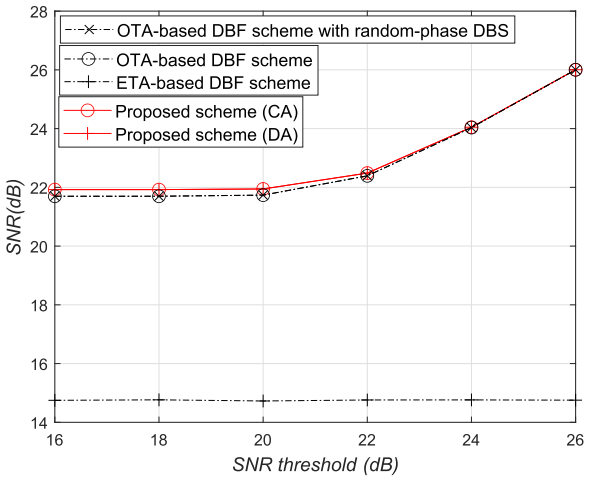

Fig. 8. The average SNR performance of different schemes versus the SNR threshold.

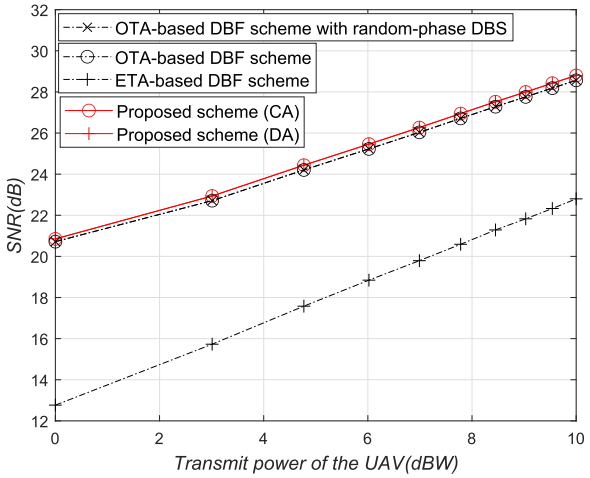

Fig. 7. The average SNR performance of different schemes versus the transmit power of the UAV.

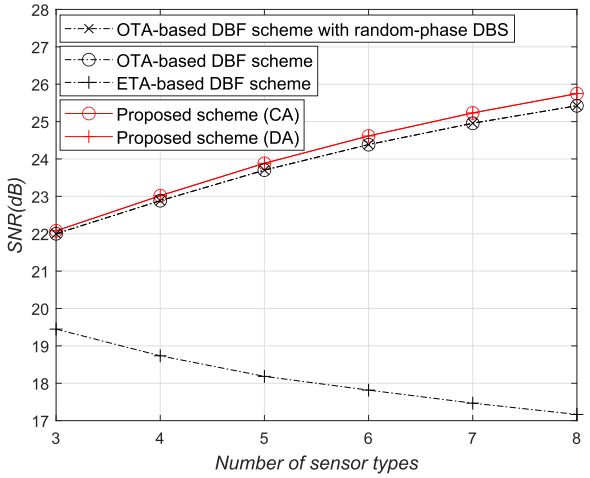

Fig. 9. The average SNR performance of different schemes versus the number of sensor types.

$N = 3$, $P_a = 5\,\text{dBW}$, $\gamma_0 = 20\,\text{dB}$, and $D_H = 20\,\text{m}$. It is observed that the proposed scheme achieves much higher SNR performance compared with the OTA-based DBF scheme with random-phase DBS, whose SNR performance is better than the OTA-based DBF scheme in the scenario of a small radius of the simulated area. This observation proves that the schemes with DBS achieve much higher SNR compared with those without DBS, especially in the situation of a small radius. The reason is that the channel gain of G2G channels drops dramatically with the increase of the radius, which results in a much lower received signal strength via indirect links.

Figure 7 shows the impact of the transmit power of the UAV on the average SNR performance in the UAV-assisted WPSN with $M = 6$, $N = 3$, $\gamma_0 = 20\,\text{dB}$, $R^{loc} = 15\,\text{m}$, and $D_H = 20\,\text{m}$. It is observed that the schemes with TA optimization (two OTA-based benchmark schemes and the proposed scheme) always meet the SNR thresholds, but the scheme without TA optimization (the ETA-based DBF scheme) may violate the SNR thresholds when the transmit power of the UAV is small. In fact, the achievable SNR of type m sensor nodes can be improved by increasing τ_0 or decreasing τ_m. However, the values of τ_0 and τ_m in schemes without TA optimization are always fixed which results in the low SNR performance. With the increase of transmit power, all schemes are able to satisfy the SNR threshold, but the proposed scheme can achieve better SNR performance as compared with benchmark schemes.

Figure 8 shows the impact of the SNR threshold on the average SNR performance in the UAV-assisted WPSN with $M = 6$, $N = 3$, $P_a = 5\,\text{dBW}$, $R^{loc} = 15\,\text{m}$, and $D_H = 20\,\text{m}$. It is observed that the SNR performance of schemes with TA optimization (two OTA-based benchmark schemes and the proposed scheme) increases as the increase of the SNR threshold. However, the scheme without TA optimization (the ETA-based DBF scheme) achieves the same SNR performance under different SNR thresholds. The reason is that the time allocation in the ETA-based DBF scheme is fixed, resulting in a fixed received SNR which may violate the SNR threshold.

Figure 9 shows the average SNR performance with different numbers of sensor types with fixed $P_a = 5\,\text{dBW}$. With the

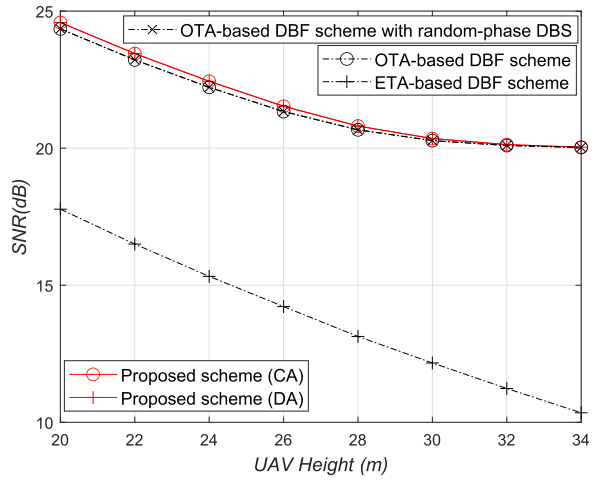

Fig. 10. The average SNR performance of different schemes versus the UAV height.

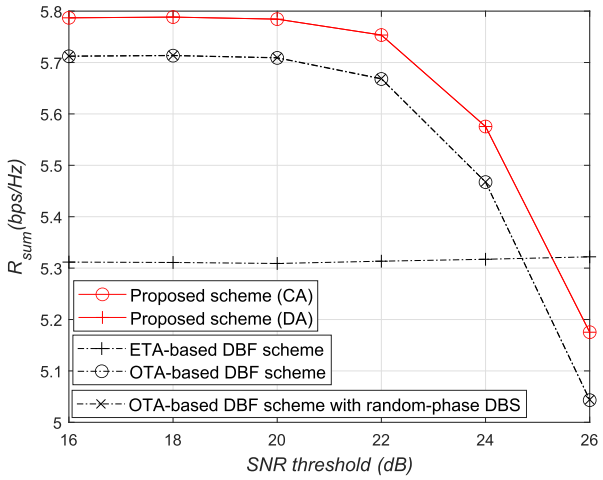

Fig. 12. The average sum-throughput performance of different schemes versus the SNR threshold.

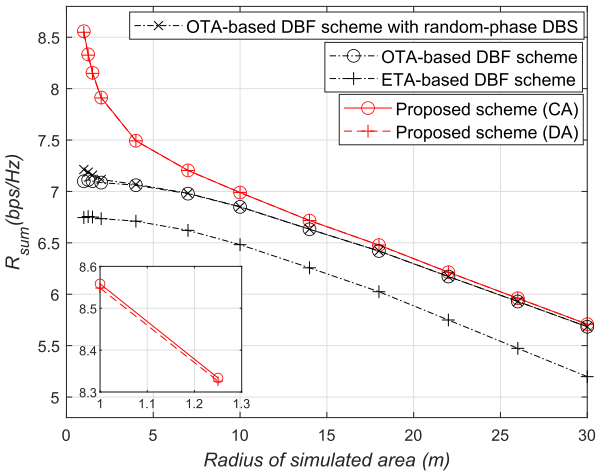

Fig. 11. The average sum-throughput performance of different schemes versus the coverage radius.

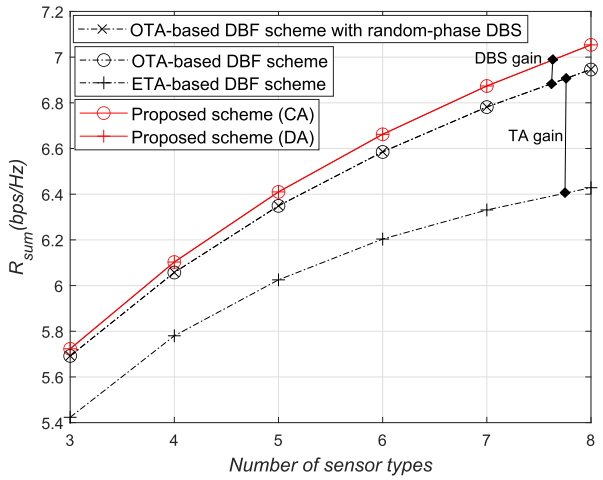

Fig. 13. The average sum-throughput performance of different schemes versus the number of sensor types.

increasing number of sensor types, there are more sensor nodes acting as backscatter nodes and less time is allocated for the WIT of each type of sensor nodes. As a result, the transmit power of sensor nodes increases, and the SNR performance of the schemes with TA optimization (two OTA-based benchmark schemes and the proposed scheme) increases. On the contrary, for the ETA-based DBF scheme, sensor nodes get lower transmit power because less time is allocated for WPT, resulting in lower SNR performance.

Figure 10 shows the impact of the UAV height on the average SNR performance with $M = 6$, $N = 3$, $P_a = 5$ dBW, $\gamma_0 = 20$ dB, and $R^{loc} = 15$ m. The average SNR performance of all schemes drops with the increase of the UAV height, but the proposed scheme achieves the maximum SNR among all schemes.

C. Sum-Throughput Performance

Figure 11 shows the impact of the radius of the simulated area R^{loc} on the average sum-throughput performance with $M = 6$, $N = 3$, $P_a = 5$ dBW, $\gamma_0 = 20$ dB, and $D_H = 20$ m. To achieve a sum-throughput objective $R_0 = 6.5$ bps/Hz, the proposed scheme can cover the sensor nodes in a circle with a radius of 17.5 m, while the ETA-based DBF scheme can only cover a circle with a radius of 9.7 m. Thus, the proposed scheme improves the coverage effectively.

Figure 12 shows the impact of the SNR threshold on the average sum-throughput performance with $M = 6$, $N = 3$, $P_a = 5$ dBW, $R^{loc} = 15$ m, and $D_H = 20$ m. It is observed that the sum-throughput performance of the schemes with TA optimization (two OTA-based benchmark schemes and the proposed scheme) drops with the increase of the SNR threshold. That is because more time is required for WPT and less time is left for WIT with the increase of the SNR threshold, resulting in lower sum-throughput performance.

By fixing $R^{loc} = 15$ m and $P_a = 5$ dBW, Fig. 13 shows the average sum-throughput comparison with different numbers of sensor types. With the increasing number of sensor types, the number of sensor nodes acting as backscatter nodes is improved and the superiorities of schemes with DBS are increasingly obvious. Accordingly, it is observed that the sum-throughput performance of the proposed scheme is

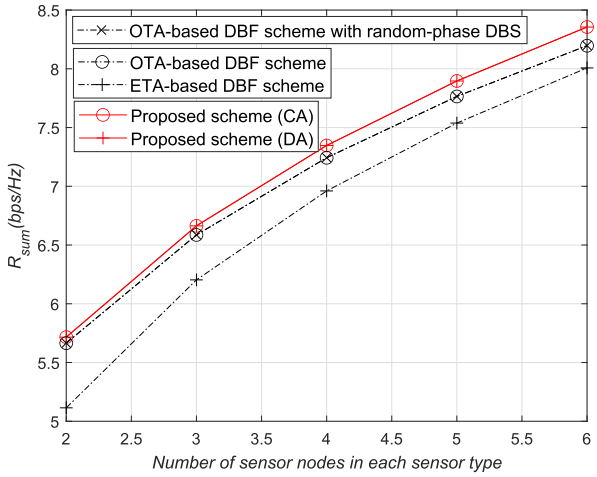

Fig. 14. The average sum-throughput performance of different schemes versus the number of sensor nodes in each sensor type.

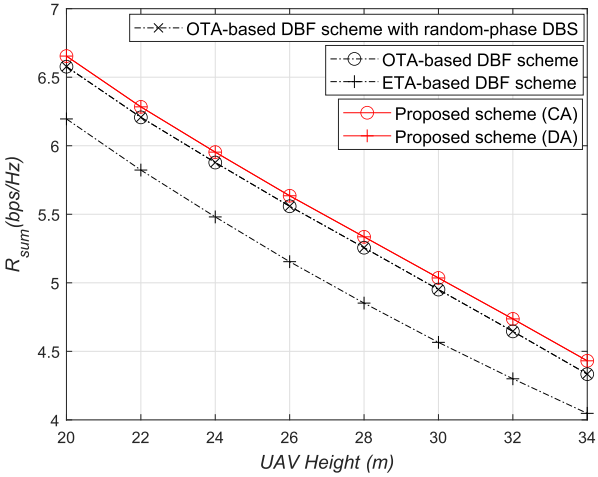

Fig. 15. The average sum-throughput performance of different schemes versus the UAV height.

increasingly better than the OTA-based DBF scheme as the number of sensor types increases. Also, the TA optimization is more important with the increase of sensor types because the time for WIT is divided into more parts. Thus, it is observed that DBS gains and TA gains are both increasingly obvious with more sensor types. By comparing the simulation results of the proposed scheme and the ETA-based DBF scheme, we can see that the proposed scheme effectively improves the sum-throughput performance and shows its superiorities in scenarios with a large number of sensor types.

Figure 14 shows the average sum-throughput performance versus the number of sensor nodes in each sensor type, where $M = 6$, $R^{loc} = 15\,\text{m}$, $P_a = 5\,\text{dBW}$, $\gamma_0 = 20\,\text{dB}$, and $D_H = 20\,\text{m}$. With the increase of the sensor nodes' number in each sensor type, the numbers of sensor nodes for DBS and DBF both increase. Thus, the improvement of the sum throughput of all schemes becomes more significant.

As shown in Fig. 15, we further study the average sum-throughput performance over UAV height D_H for different transmission schemes, where $M = 6$, $N = 3$, $R^{loc} = 15\,\text{m}$, $P_a = 5\,\text{dBW}$, and $\gamma_0 = 20\,\text{dB}$. It is observed that the sum throughput of all schemes drops with the increase of UAV height because of the higher pathloss, but the proposed scheme still outperforms other schemes with different UAV heights.

VII. Conclusion

In this paper, we have investigated a UAV-assisted WPSN with multiple types of sensor nodes. A joint distributed beamforming and backscattering scheme has been designed to enhance the transmission performance from sensor nodes to the UAV. A two-step algorithm has been proposed to maximize the sum throughput. Simulation results have been provided to demonstrate the superiority of the proposed scheme as compared to benchmark schemes, especially in scenarios with a large number of sensor nodes. The proposed transmission scheme can effectively enhance the long-distance transmission performance, which is of critical importance for UAV-aided IoT scenarios. For the future work, we will investigate the group size optimization problem for distributed beamforming considering intragroup information synchronization cost.

Appendix A
Proof for Lemma 1

It is assumed that there is an SNR value γ_m higher than γ_i, $\forall i \in \{1, 2, \cdots, m-1, m+1, \cdots, M\}$ when the optimal TA solution of problem P1.1 is achieved. Since

$$\frac{\partial R_m}{\partial \tau_m}(\tau_m) = \frac{1}{\ln 2}\left(\ln\left(1+\gamma'_m\frac{\tau_0}{\tau_m}\right) - \frac{\gamma'_m\frac{\tau_0}{\tau_m}}{1+\gamma'_m\frac{\tau_0}{\tau_m}}\right) \quad (38)$$

is monotonically decreasing over τ_m and $\frac{\partial R_m}{\partial \tau_m}(+\infty) = 0$, $\frac{\partial R_m}{\partial \tau_m}(\tau_m) > 0$ holds for $\tau_m \in (0, 1]$. R_m is monotonically increasing over τ_m. The above equation can be rewritten as

$$\frac{\partial R_m}{\partial \tau_m}(\gamma_m) = \frac{1}{\ln 2}\left(\ln(1+\gamma_m) - \frac{\gamma_m}{1+\gamma_m}\right), \quad (39)$$

where $\frac{\partial R_m}{\partial \tau_m}(\gamma_m)$ is monotonically increasing over γ_m. If there is an SNR value γ_m higher than γ_i, we have

$$dR_m = \frac{\partial R_m}{\partial \tau_m}(\gamma_m)d\tau \;<\; dR_i = \frac{\partial R_i}{\partial \tau_i}(\gamma_i)d\tau_i. \quad (40)$$

For a given τ_0, the above equation means that the sum throughput can be improved by saving a small enough time duration $d\tau$ from the sensor nodes of the other sensor types to the type m sensor nodes for WIT. Then, γ_m decreases while γ_i increases. Finally, all $\gamma_m, \forall m \in \{1, 2, \cdots, M\}$ will obtain a common SNR that contradicts the original assumption. To sum up, the original assumption fails and the proof is complete.

References

[1] Z. Mao, F. Hu, Q. Li, W. Wu, and X. S. Shen, "Joint distributed beamforming and backscatter cooperation for UAV-assisted WPSNs," in *Proc. IEEE Global Commun. Conf. (GLOBECOM)*, Dec. 2021, pp. 1–6.

[2] X. Shen, J. Gao, W. Wu, M. Li, C. Zhou, and W. Zhuang, "Holistic network virtualization and pervasive network intelligence for 6G," *IEEE Commun. Surveys Tuts.*, vol. 24, no. 1, pp. 1–30, 1st Quart., 2022.

[3] H. Liu, F. Hu, S. Qu, Z. Li, and D. Li, "Multipoint wireless information and power transfer to maximize sum-throughput in WBAN with energy harvesting," *IEEE Internet Things J.*, vol. 6, no. 4, pp. 7069–7078, Aug. 2019.

[4] L. Xie, J. Xu, and Y. Zeng, "Common throughput maximization for UAV-enabled interference channel with wireless powered communications," *IEEE Trans. Commun.*, vol. 68, no. 5, pp. 3197–3212, May 2020.
[5] C. Zhou *et al.*, "Deep reinforcement learning for delay-oriented IoT task scheduling in SAGIN," *IEEE Trans. Wireless Commun.*, vol. 20, no. 2, pp. 911–925, Feb. 2021.
[6] H. Ju and R. Zhang, "Throughput maximization in wireless powered communication networks," *IEEE Trans. Wireless Commun.*, vol. 13, no. 1, pp. 418–428, Jan. 2013.
[7] H. Wu, F. Lyu, C. Zhou, J. Chen, L. Wang, and X. Shen, "Optimal UAV caching and trajectory in aerial-assisted vehicular networks: A learning-based approach," *IEEE J. Sel. Areas Commun.*, vol. 38, no. 12, pp. 2783–2797, Dec. 2020.
[8] W. Wu *et al.*, "AI-native network slicing for 6G networks," *IEEE Wireless Commun.*, vol. 29, no. 1, pp. 96–103, Feb. 2022.
[9] J. Xu, Y. Zeng, and R. Zhang, "UAV-enabled wireless power transfer: Trajectory design and energy optimization," *IEEE Trans. Wireless Commun.*, vol. 17, no. 8, pp. 5092–5106, Aug. 2018.
[10] R. Zhang, M. Wang, L. X. Cai, and X. Shen, "Learning to be proactive: Self-regulation of UAV based networks with UAV and user dynamics," *IEEE Trans. Wireless Commun.*, vol. 20, no. 7, pp. 4406–4419, Jul. 2021.
[11] J. Baek, S. I. Han, and Y. Han, "Optimal UAV route in wireless charging sensor networks," *IEEE Internet Things J.*, vol. 7, no. 2, pp. 1327–1335, Feb. 2020.
[12] Z. Xiao, H. Dong, L. Bai, D. O. Wu, and X.-G. Xia, "Unmanned aerial vehicle base station (UAV-BS) deployment with millimeter-wave beamforming," *IEEE Internet Things J.*, vol. 7, no. 2, pp. 1336–1349, Feb. 2020.
[13] Y. Liu, K. Xiong, Q. Ni, P. Fan, and K. B. Letaief, "UAV-assisted wireless powered cooperative mobile edge computing: Joint offloading, CPU control, and trajectory optimization," *IEEE Internet Things J.*, vol. 7, no. 4, pp. 2777–2790, Apr. 2020.
[14] T. Shen and H. Ochiai, "A UAV-enabled wireless powered sensor network based on NOMA and cooperative relaying with altitude optimization," *IEEE Open J. Commun. Soc.*, vol. 2, pp. 21–34, 2021.
[15] S. Suman, S. Kumar, and S. De, "UAV-assisted RFET: A novel framework for sustainable WSN," *IEEE Trans. Green Commun. Netw.*, vol. 3, no. 4, pp. 1117–1131, Dec. 2019.
[16] X. Shen *et al.*, "AI-assisted network-slicing based next-generation wireless networks," *IEEE Open J. Veh. Technol.*, vol. 1, pp. 45–66, 2020.
[17] L. Yang and W. Zhang, "Beam tracking and optimization for UAV communications," *IEEE Trans. Wireless Commun.*, vol. 18, no. 11, pp. 5367–5379, Nov. 2019.
[18] X. Yuan, T. Yang, Y. Hu, J. Xu, and A. Schmeink, "Trajectory design for UAV-enabled multiuser wireless power transfer with nonlinear energy harvesting," *IEEE Trans. Wireless Commun.*, vol. 20, no. 2, pp. 1105–1121, Feb. 2021.
[19] R. Mudumbai, D. R. B. Iii, U. Madhow, and H. V. Poor, "Distributed transmit beamforming: Challenges and recent progress," *IEEE Commun. Mag.*, vol. 47, no. 2, pp. 102–110, Feb. 2009.
[20] X. Li, C. You, S. Andreev, Y. Gong, and K. Huang, "Wirelessly powered crowd sensing: Joint power transfer, sensing, compression, and transmission," *IEEE J. Sel. Areas Commun.*, vol. 37, no. 2, pp. 391–406, Feb. 2019.
[21] W. Wu, N. Cheng, N. Zhang, P. Yang, W. Zhuang, and X. Shen, "Fast mmWave beam alignment via correlated bandit learning," *IEEE Trans. Wireless Commun.*, vol. 18, no. 12, pp. 5894–5908, Dec. 2019.
[22] S. Gong, X. Huang, J. Xu, W. Liu, P. Wang, and D. Niyato, "Backscatter relay communications powered by wireless energy beamforming," *IEEE Trans. Commun.*, vol. 66, no. 7, pp. 3187–3200, Jul. 2018.
[23] W. Chen, H. Ding, S. Wang, D. B. da Costa, F. Gong, and P. H. Juliano Nardelli, "Backscatter cooperation in NOMA communications systems," *IEEE Trans. Wireless Commun.*, vol. 20, no. 6, pp. 3458–3474, Jun. 2021.
[24] R. Han, L. Bai, Y. Wen, J. Liu, J. Choi, and W. Zhang, "UAV-aided backscatter communications: Performance analysis and trajectory optimization," *IEEE J. Sel. Areas Commun.*, vol. 39, no. 10, pp. 3129–3143, Oct. 2021.
[25] L. Xie, X. Cao, J. Xu, and R. Zhang, "UAV-enabled wireless power transfer: A tutorial overview," *IEEE Trans. Green Commun. Netw.*, vol. 5, no. 4, pp. 2042–2064, Dec. 2021.
[26] C. Zhan *et al.*, "Completion time and energy optimization in the UAV-enabled mobile-edge computing system," *IEEE Internet Things J.*, vol. 7, no. 8, pp. 7808–7822, Aug. 2020.
[27] L. Gupta, R. Jain, and G. Vaszkun, "Survey of important issues in UAV communication networks," *IEEE Commun. Surveys Tuts.*, vol. 18, no. 2, pp. 1123–1152, 2nd Quart., 2016.
[28] Z. Liu, C. Zhan, Y. Cui, C. Wu, and H. Hu, "Robust edge computing in UAV systems via scalable computing and cooperative computing," *IEEE Wireless Commun.*, vol. 28, no. 5, pp. 36–42, Oct. 2021.
[29] S. Zhang, H. Zhang, and L. Song, "Beyond D2D: Full dimension UAV-to-everything communications in 6G," *IEEE Trans. Veh. Technol.*, vol. 69, no. 6, pp. 6592–6602, Apr. 2020.
[30] K. Zhu *et al.*, "Aerial refueling: Scheduling wireless energy charging for UAV enabled data collection," *IEEE Trans. Green Commun. Netw.*, vol. 6, no. 3, pp. 1494–1510, Sep. 2022.
[31] H. Yan, Y. Chen, and S.-H. Yang, "UAV-enabled wireless power transfer with base station charging and UAV power consumption," *IEEE Trans. Veh. Technol.*, vol. 69, no. 11, pp. 12883–12896, Nov. 2020.
[32] H.-T. Ye, X. Kang, J. Joung, and Y.-C. Liang, "Optimization for wireless-powered IoT networks enabled by an energy-limited UAV under practical energy consumption model," *IEEE Wireless Commun. Lett.*, vol. 10, no. 3, pp. 567–571, Mar. 2021.
[33] Y. Yu, J. Tang, J. Huang, X. Zhang, D. K. C. So, and K.-K. Wong, "Multi-objective optimization for UAV-assisted wireless powered IoT networks based on extended DDPG algorithm," *IEEE Trans. Commun.*, vol. 69, no. 9, pp. 6361–6374, Sep. 2021.
[34] D.-T. Do, A.-T. Le, Y. Liu, and A. Jamalipour, "User grouping and energy harvesting in UAV-NOMA system with AF/DF relaying," *IEEE Trans. Veh. Technol.*, vol. 70, no. 11, pp. 11855–11868, Nov. 2021.
[35] I. Ahmad, C. K. Sung, D. Kramarev, G. Lechner, H. Suzuki, and I. Grivell, "Outage probability and ergodic capacity of distributed transmit beamforming with imperfect CSI," *IEEE Trans. Veh. Technol.*, vol. 71, no. 3, pp. 3008–3019, Mar. 2022.
[36] J. Xu, Z. Zhong, and B. Ai, "Wireless powered sensor networks: Collaborative energy beamforming considering sensing and circuit power consumption," *IEEE Wireless Commun. Lett.*, vol. 5, no. 4, pp. 344–347, Aug. 2016.
[37] T. Feng, L. Xie, J. Yao, and J. Xu, "UAV-enabled data collection for wireless sensor networks with distributed beamforming," *IEEE Trans. Wireless Commun.*, vol. 21, no. 2, pp. 1347–1361, Feb. 2021.
[38] B. Lyu, Z. Yang, H. Guo, F. Tian, and G. Gui, "Relay cooperation enhanced backscatter communication for Internet-of-Things," *IEEE Internet Things J.*, vol. 6, no. 2, pp. 2860–2871, Apr. 2019.
[39] H. Ochiai, P. Mitran, H. V. Poor, and V. Tarokh, "Collaborative beamforming for distributed wireless ad hoc sensor networks," *IEEE Trans. Signal Process.*, vol. 53, no. 11, pp. 4110–4124, Nov. 2005.
[40] J. Meredith, *Study on Enhanced LTE Support for Aerial Vehicles*, Sophia Antipolis, France, 3GPP, document TR 36, 2017.
[41] *Study on LTE Device to Device Proximity Services: Radio Aspects*, 3GPP document TR 36.843 V12. 0.0, 2014.
[42] E. Boshkovska, D. W. K. Ng, N. Zlatanov, A. Koelpin, and R. Schober, "Robust resource allocation for MIMO wireless powered communication networks based on a non-linear EH model," *IEEE Trans. Commun.*, vol. 65, no. 5, pp. 1984–1999, May 2017.
[43] S. Boyd and L. Vandenberghe, *Convex Optimization*. Cambridge, U.K.: Cambridge Univ. Press, 2004.
[44] E. Höpfinger, "On the solution of the unidimensional local minimization problem," *J. Optim. Theory Appl.*, vol. 18, no. 3, pp. 425–428, 1976.
[45] S. H. Mousavi, J. Haghighat, and W. Hamouda, "A relay subset selection scheme for wireless sensor networks based on channel state information," in *Proc. IEEE Int. Conf. Commun. (ICC)*, May 2016, pp. 1–6.
[46] G. Li, D. Mishra, Y. Hu, Y. Huang, and H. Jiang, "Adaptive relay selection strategies for cooperative NOMA networks with user and relay cooperation," *IEEE Trans. Veh. Technol.*, vol. 69, no. 10, pp. 11728–11742, Oct. 2020.

Zhi Mao (Member, IEEE) received the B.S. degree in communication engineering from the Changchun University of Science and Technology, Changchun, Jilin, China, in 2017, and the Ph.D. degree from the College of Communication Engineering, Jilin University, Changchun, in 2022. His current research interests include resource allocation and network optimization in 802.11 PHY protocol design.

Fengye Hu (Senior Member, IEEE) received the B.S. degree from the Department of Precision Instrument, Xian University of Technology, China, in 1996, and the M.S. and Ph.D. degrees in communication and information systems from Jilin University, China, in 2000 and 2007, respectively.

He was a Visiting Scholar in electrical and electronic engineering from Nanyang Technological University (NTU), Singapore, in 2011. He is currently a Full Professor with the College of Communication Engineering, Jilin University. His current research interests include wireless body area networks, wireless energy and information transfer, energy harvesting, cognitive radio, and space–time communication. He has published 50 publications in IEEE journals and conferences. He organized the first and second Asia-Pacific Workshop on Wireless Networking and Communications (APWNC 2013 and APWNC 2015). He also organized the Future 5G Forum on Wireless Communications and Networking Big Data (FWCN 2016). He was an Executive Co-Chairs of IEEE/CIC International Conference on Communications in China (ICCC), China, in 2019. He is the Editor of *IET Communications* and *China Communications*, and is the Editor of *Physical Communication on Special Issue on Ultra-Reliable, Low-Latency and Low-Power Transmissions in the Era of Internet-of-Things*.

Wen Wu (Senior Member, IEEE) received the B.E. degree in information engineering from the South China University of Technology, Guangzhou, China, and the M.E. degree in electrical engineering from the University of Science and Technology of China, Hefei, China, in 2012 and 2015, respectively, and the Ph.D. degree in electrical and computer engineering from the University of Waterloo, Waterloo, ON, Canada, in 2019. He was a Post-Doctoral Fellow at the Department of Electrical and Computer Engineering, University of Waterloo. He is currently an Associate Researcher with the Frontier Research Center, Peng Cheng Laboratory, Shenzhen, China. His research interests include 6G networks, network intelligence, and network virtualization.

Huaqing Wu (Member, IEEE) received the B.E. and M.E. degrees from the Beijing University of Posts and Telecommunications, Beijing, China, in 2014 and 2017, respectively, and the Ph.D. degree from the University of Waterloo, Ontario, Canada, in 2021. She was a Post-Doctoral Fellow at the Department of Electrical and Computer Engineering, MacMaster University, from 2021 to 2022. She is currently an Assistant Professor with the Department of Electrical and Software Engineering, University of Calgary, Alberta, Canada. Her current research interests include B5G/6G, space-air-ground integrated networks, the Internet of Vehicles, edge computing/caching, and artificial intelligence (AI) for future networking. She was a recipient of the prestigious Natural Sciences and Engineering Research Council of Canada (NSERC) Postdoctoral Fellowship Award in 2021 and the Best Paper Award at IEEE GLOBECOM 2018 and Chinese Journal on Internet of Things 2020.

Xuemin (Sherman) Shen (Fellow, IEEE) received the Ph.D. degree in electrical engineering from Rutgers University, New Brunswick, NJ, USA, in 1990.

He is an University Professor with the Department of Electrical and Computer Engineering, University of Waterloo, Canada. His research interests include network resource management, wireless network security, the Internet of Things, 5G and beyond, and vehicular ad hoc and sensor networks. He is a registered Professional Engineer of Ontario, Canada, an Engineering Institute of Canada Fellow, a Canadian Academy of Engineering Fellow, a Royal Society of Canada Fellow, a Chinese Academy of Engineering Foreign Member, and a Distinguished Lecturer of the IEEE Vehicular Technology Society and Communications Society. He received the Premier's Research Excellence Award (PREA) in 2003 from the Province of Ontario, Canada and the Excellent Graduate Supervision Award in 2006 from the University of Waterloo. He has also received the Technical Recognition Award from the AHSN Technical Committee in 2013, the Joseph LoCicero Award in 2015, and Wireless Communications Technical Committee in 2019; the Education Award in 2017 from the IEEE Communications Society (ComSoc); the James Evans Avant Garde Award in 2018 from the IEEE Vehicular Technology Society; the R.A. Fessenden Award in 2019 from IEEE, Canada; the Award of Merit from the Federation of Chinese Canadian Professionals (Ontario) in 2019; and the Canadian Award for Telecommunications Research from the Canadian Society of Information Theory (CSIT) in 2021. He was the Technical Program Committee Chair/Co-Chair for IEEE Globecom'16, IEEE Infocom'14, IEEE VTC'10 Fall, IEEE Globecom'07, and the Chair for the IEEE ComSoc Technical Committee on Wireless Communications. He is the President Elect of the IEEE ComSoc. He was the Vice President for Technical and Educational Activities, the Vice President of Publications, the Member-at-Large on the Board of Governors, the Chair of the Distinguished Lecturer Selection Committee, and a member of IEEE Fellow Selection Committee of the ComSoc. He was the Editor-in-Chief of the IEEE INTERNET OF THINGS JOURNAL, *IEEE Network*, and *IET Communications*.